Supplemental Material for: Photoinduced Dynamics at the Water/TiO_2(101) Interface

Michael Wagstaffe,[1,*] Adrian Dominguez-Castro,[2] Lukas Wenthaus,[3] Steffen Palutke,[3] Dmytro Kutnyakhov,[3] Michael Heber,[3] Federico Pressacco,[3] Siarhei Dziarzhytski,[3] Helena Gleißner,[4,5,6] Verena Kristin Gupta,[2] Harald Redlin,[3] Adriel Dominguez,[2,7,8,9] Thomas Frauenheim,[2,7,8] Angel Rubio,[10,9,11,12] Andreas Stierle,[4,5,6,†] and Heshmat Noei[4,6]

[1] *Centre for X-ray and Nano Science CXNS, Deutsches Elektronen-Synchrotron DESY, Notkestr. 85, 22607 Hamburg, Germany*

[2] *Bremen Center for Computational Materials Science, University of Bremen, Am Fallturm 1, 28359 Bremen, Germany*

[3] *Deutsches Elektronen-Synchrotron DESY, Notkestr. 85, 22607 Hamburg, Germany*

[4] *Center for X-ray and Nano Science CXNS, Deutsches Elektronen-Synchrotron DESY, Notkestr. 85, 22607 Hamburg, Germany*

[5] *Universität Hamburg, Fachbereich Physik, Jungiusstr. 9-11, 20355 Hamburg, Germany*

[6] *The Hamburg Centre for Ultrafast Imaging, Universität Hamburg, Luruper Chaussee 149, 22761 Hamburg, Germany*

[7] *Computational Science and Applied Research Institute (CSAR), 518110, Shenzhen, China*

[8] *Beijing Computational Science Research Center (CSRC), 100193, Beijing, China*

[9] *Nano-Bio Spectroscopy Group, Departamento de Fisica de Materiales, Universidad del País Vasco, UPV/EHU- 20018 San Sebastián, Spain*

[10] *Center for Free-Electron Laser Science CFEL, Deutsches Elektronen-Synchrotron DESY, Notkestr. 85, 22607 Hamburg, Germany*

[11] *Max Planck Institute for the Structure and Dynamics of Matter, Luruper Chaussee 149, 22761 Hamburg, Germany*

[12] *Center for Computational Quantum Physics, Flatiron Institute, NY 10010, New York, USA*

(Dated: February 10, 2023)

S1: Experimental Method and Computational Details

EXPERIMENTAL METHOD

The experiment was performed at the second branch of the plane grating monochromator beamline PG2[1, 2] of the free-electron laser facility FLASH located at Deutsches Elektronen-Synchrotron (DESY) in Hamburg, Germany[3, 4]. To measure core level XP spectra FLASH was operated with a fundamental wavelength of 5.74 nm (216 eV) and an average pulse energy of 30 - 40 μJ. By tuning the monochromator the 3rd harmonic of FLASH, radiation of 1.91 nm (647.9 eV), could be used for the experiment. The FEL provided a pulse pattern of bursts with 10 Hz repetition rate. Each burst consists of 400 single soft X-ray pulses separated by 1 μs (a repetition rate of 1 MHz) giving an effective pulse rate of 4000 pulses/s. Each FEL pulse had a pulse length < 150 fs including monochromator dispersion. An optical laser of 770 nm (1.6 eV) providing the same pulse pattern as the FEL was used to pump the photocatalytic reaction via two-photon excitation. With a pulse energy of 20 μJ and a spot size of ca. 300 μm the laser fluence on the sample was 22 mJ/cm^2. The pulses of the optical laser had a duration less than 120 fs and were synchronized to the FEL pulses with a jitter in the range of 150 fs FWHM. The timing offset of the optical pulses with respect to the FEL pulses was controlled by a mechanical delay stage. Two-photon excitation was employed to maximise comparability to previous studies[5]. Watanabe and Hayashi utilized time-resolved spectroscopy to monitor the time response of the self-trapped exciton luminescence in anatase and compared the charge carrier dynamics for excitons produced via single-photon and double photon ionization.[6] Observing a similar behavior for both systems, it was concluded that the carrier separation is ascribed to intrinsic dynamical properties of photocarriers in anatase. As such, utilizing two-photon absorption as opposed to single photon absorption to generate the electrons/holes should not influence the subsequent photo-dynamics and therefore the understanding of the photocatalytic process. Neither X-ray nor optical induced beam damage was observed, confirmed by the absence of any long-term shift in the position of the lattice oxide peak throughout the experiments, as shown below recorded over the period of around an hour during exposure to both pump and probe lasers ($h\nu_{FEL} = 645$ eV, $h\nu_{opt} = 1.6$ eV, T = 295 K). No peak shifts or other changes are observed that might be expected following the formation of defects that could be induced by the laser,

as has been previously reported in similar experiments.[7] The right plot shows two parts of the XP map displayed as 2D core-level spectra from the O 1s core level taken from the beginning and the end of the time window. No discernible changes are present. Furthermore, static Ti 2p spectra recorded at regular intervals reiterated that no additional Ti^{3+} species formed.

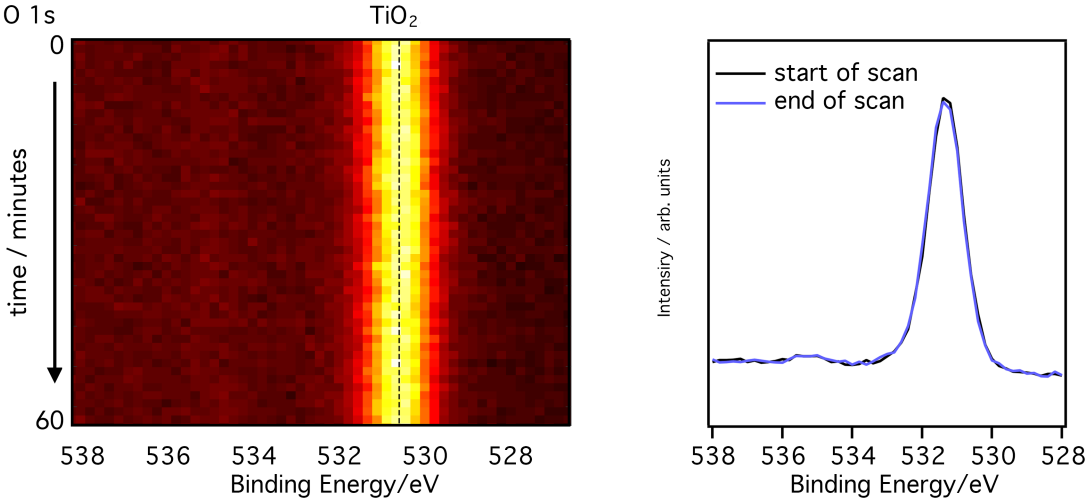

The experimental (ultra-high vacuum) high efficient wide-angle electron spectrometer WESPE chamber[8] was equipped with a heating stage and an ion gun for sample preparation, low energy electron diffraction (LEED) optics and a Themis 1000 high-resolution time of flight spectrometer equipped with a three-dimensional delay line detector (Surface Concept 3D-DLD4040-4Q). The manipulator contained a cryostat, allowing the sample to be cooled with liquid He. There were two gas lines containing Ar (purity 99.999%) and O_2 (purity 99.999%) for sample preparation and a glass vial mounted on the chamber containing H_2O which was thoroughly freeze-pump-thawed prior to surface exposure. The anatase TiO_2(101) single crystal (8 mm x 8 mm x 2 mm) was prepared by repeated 1 keV Ar^+ ion bombardment and 850 K anneal cycles, in a backpressure of 1 x 10^{-8} mbar O_2, until X-ray photoelectron spectra showed the surface to be free of contamination and a sharp (1x1) LEED pattern was obtained. For the final annealing step, the sample was left to cool in the back pressure of O_2 before being exposed to H_2O (5 x 10^{-8} mbar); this treatment produced the stoichiometric surface as evidenced by the absence of any Ti^{3+} species in the Ti 2p spectrum, which can usually be inferred from a low BE shoulder to the Ti^{4+} doublet[9], shown in the figure below.

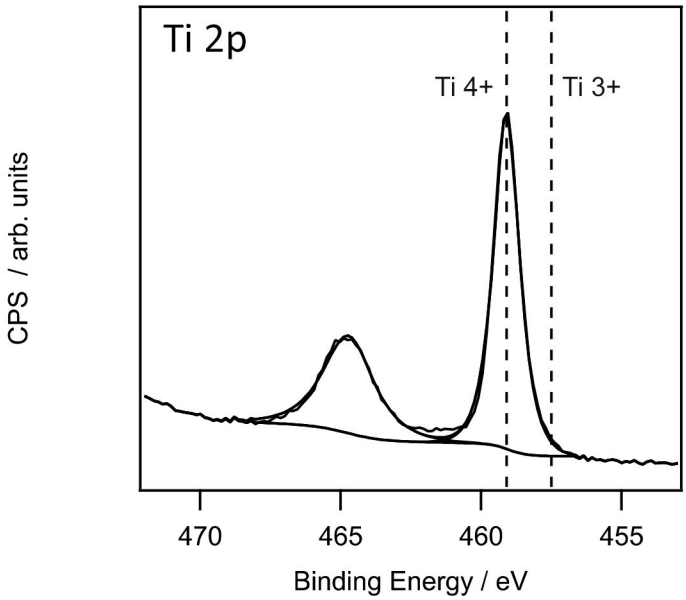

The figure showing the Ti 2p spectrum contains time averaged data ($h\nu_{FEL}$ = 645 eV, $h\nu_{opt}$ = 1.6 eV, T = 295 K) following sample preparation, highlighting the absence of Ti^{3+} species.

This surface was chosen since anatase is the majority polymorph in Degussa P25 TiO_2 powder and has a higher photocatalytic activity when compared to rutile[9]. The (101) surface termination is the most stable, constituting a significant portion of the exposed surface area in nanostructured materials[10], making it the most appropriate surface to study when modelling photocatalytic systems. All spectra, unless otherwise stated, were recorded at normal emission, at 160 K and with a 20 eV pass energy. Fitting of the XP spectra was carried out using CasaXPS, either with a shirley or a linear background in conjunction with Gaussian:Lorentzian(G:L) curves (0.7:0.3) to simulate the line shapes. To align the data on the BE scale the work function of the analyzer was calculated by aligning the Ti 2p peak to 459.1 eV, which was subsequently used to calculate the binding energies of the O 1s core level peaks.

COMPUTATIONAL DETAILS

For the correct description of the electronic structure, adsorption properties on the TiO_2 anatase surface, and for the study of the evolution of the density matrix using real time propagation to compute absorption spectra and Ehrenfest dynamics, the DFTB+ code is

used[11].

The present study is performed in periodic conditions with 108 atoms and lattice parameters: a = 11.3313 Å, b = 10.1715 Å and c = 30.0000 Å for the unit cell of the TiO_2 anatase(101) surface. For the choice of k-points, sampling of a (4x4x1) Monkhorst-Pack set is employed. To increase the accuracy of the description of the Hydrogen bonds, the matorg parameter set as referred to by Di Valenti et al.[12] and a hydrogen bonding damping (HBD) function equal to 4 are used. To model the dissociative adsorption an OH group is placed above a Ti_{5c} site and a proton H at a O_{2c} site.

The adsorption energies, E_{ads} were calculated by:

$E_{ads} = \frac{1}{n}(E_{complex} - E_{TiO_2} - E_{H_2O})$

where $E_{complex}$, E_{TiO_2}, E_{H_2O} are the total energies of the water-TiO_2 complex formed by the water-TiO_2 anatase(101) surface, the TiO_2 anatase(101) surface and the water molecule respectively and n is the number of water molecules. Within this definition for adsorption energy, a negative value indicates an exothermic process.

To obtain the absorption spectra, an initial perturbation to the initial ground-state matrix is introduced. This perturbation has the shape of a Dirac delta pulse, and the density matrix evolves in time, and its evolution can be resolved by time integration of the Liouville-von Newmann equation of motion. An initial electric field value of 0.001 V/Å is used. In order to model the dynamics of an electromagnetic wave, a $\sin^2$ shaped pulse is employed describing the electron dynamics during the light absorption with an electric field of 0.1 V/Å and an laser of wavelength 382 nm (3.245 eV). The total duration of the pulse is 20 fs in all cases. For the nuclei evolution in the Ehrenfest dynamics based on the Verlet algorithm a Temperature of 160 K is used. The employed method had been used with success in previous studies[13, 14].

The VASP code[15–18] has been employed to calculate the expected binding energies for species relevant to our system in the O 1s core level before and after light illumination. Calculations were carried out at the Γ point and using PBE functional[19] with an energy cutoff of 450 eV and the projected augmented-wave method[20, 21]. To calculate the core level energies the Slater transition state approach was selected.

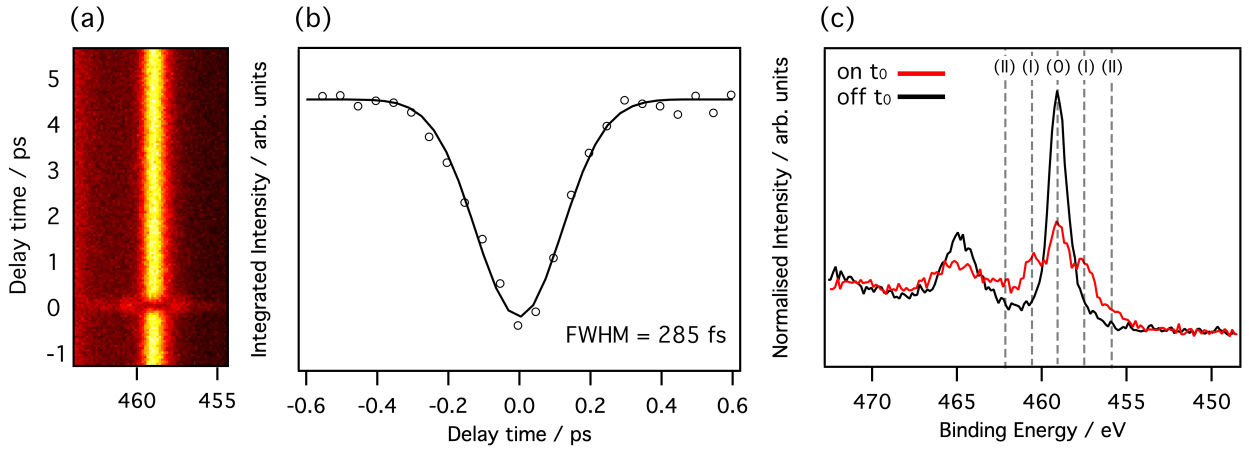

S2: Figure S2(a) shows the Ti 2p core level XP spectra ($h\nu_{FEL}$ = 645 eV, $h\nu_{opt}$ = 1.6 eV, T = 295 K) as a function of delay time. The counts over the Ti $2p_{3/2}$ component were integrated and plotted against delay time in (b). A noticeable reduction in intensity can be seen at, our hereinafter defined value of, 0 ps. This is indicative of time zero[22] and occurs due to the formation of sidebands resulting from the interaction of the intense optical field from the laser with the emitted X-ray induced photoelectrons. Figure (c) shows the Ti 2p spectra extracted in a 300 fs window corresponding to a time off time zero (black) and on time zero (red). Side bands shifted by ± 1.6 eV, labeled (I), are clearly observed. Side-bands of 2^{nd} order, labeled (II), suggest that two-pump-photon absorption/emission occurs

These data allow the temporal overlap between the free-electron laser and optical laser pulses to be determined by using the process of laser-assisted photoemission to monitor the creation and decay of sidebands in the time-dependent photoelectron signal, as described in [22]. Doing so determines the temporal resolution of the experiment and corresponds to the time at which the FEL pulse and the optical laser pulse simultaneously arrive at the sample. This was carried out on the as-prepared surface using a 22 mJ/cm^2 770 nm laser. Fitting a Gaussian curve to the integrated intensity of the Ti $2p_{3/2}$ peak as a function of time, (b), yields a fit with a FWHM of 285 ± 9 fs.

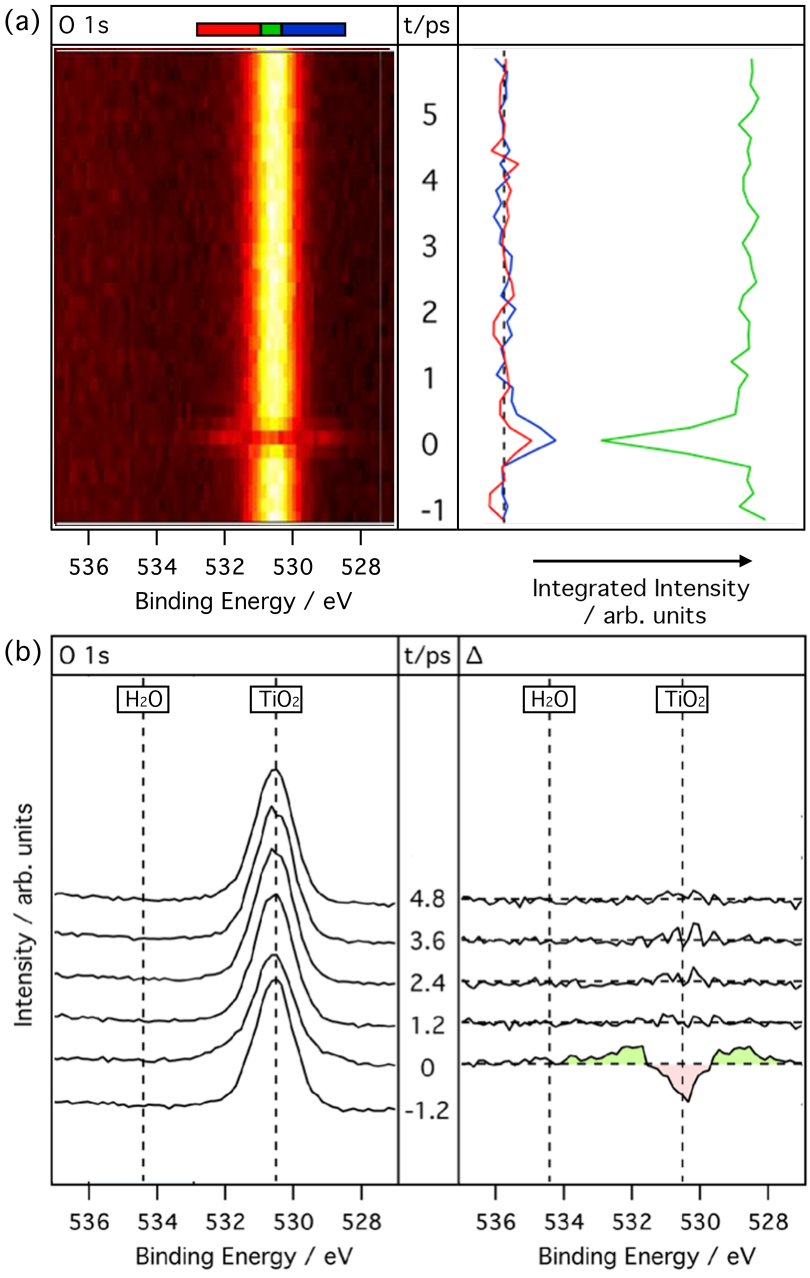

S3: Time resolved XP spectra for the as-prepared TiO_2(101) system without H_2O(hν_{FEL} = 645 eV, hν_{opt} = 1.6 eV, T = 295 K). To study the photoinduced dynamics, the O 1s core level was selected. Here both the substrate and adsorbate related peaks could be monitored simultaneously with maximum surface sensitivity[23]; with an estimated sampling depth, 3λ (where λ is the photoelectron mean free path), of less than 2 nm[24]. Figure (a) shows the time-resolved O1s XPS map recorded during the pump probe experiment between -1.0 ps and 6.0 ps following photoexcitation (with a temporal resolution of 285 fs), to the right is an integrated intensity plot, as a function of delay time, in which the colours correspond to

the regions marked on the XPS map. (b) O 1s core level spectra from (a) averaged over 1.2 ps windows with corresponding difference spectra taken from the pre-pumped region at -1.2 ps to highlight any time induced changes. At 0 ps the formation of side bands is clearly visible as expected. Following this change no additional changes are observed. The peak position remains constant and no broadening takes place.

When electron-hole pairs are generated in a photocatalytic system one must consider the effect of the surface photovoltage (SPV), which acts to restore the system back to a flat band condition.[7] This can be defined as the illumination induced change in the surface potential due to the redistribution of charge in the near surface region.[25] This will influence the extent of band bending in the system as long as photogenerated charge carriers are present, i.e. depending on the recombination time of the system.[7, 26] When a semiconductor is exposed to light of sufficient energy, the absorbed photons will generate electron–hole pairs via band-to-band transitions. These electron-hole pairs will then separate as the charge carriers move in opposite directions due to the electric field that is induced in the bent band region. This essentially neutralises built up charge and moves the system back to a flat band condition. [25] This effect can be monitored using photoelectron spectroscopy by observing the decay of the peak shift induced by band bending in the substrate related core level spectra. Ozawa et al.[7] investigated the relaxation times of charge carriers photogenerated on anatase and rutile TiO_2 by monitoring this shift in a time-resolved pump probe photoemission study (similarly utilising two-photon excitation) and reported that upon pump laser irradiation (12 mJ/cm^2/pulse, 3.06 eV) of as-prepared TiO_2 both the O 1s and the Ti 2p core level spectra exhibit red shifts to lower binding energies of up to 0.2 eV. Since the SPV energy shift always acts to diminish intrinsic band bending, this negative binding energy shift can be seen as a movement from downwards-bent bands (typical for vacuum prepared anatase(101)[9, 27, 28]) to the flat band condition. Similarly, Zhang et al.[29] studied charge carrier dynamics on hydroxylated single crystal rutile TiO_2(110) by probing the relevant regions surrounding the Fermi edge. They observed a redistribution of occupied states due to the movement of photogenerated charge carriers and the subsequent ultrafast trapping thereof. Furthermore, they observed a subtle binding energy shift of 10 meV to lower energies, which was attributed to SPV induced effects leading to a relaxation of the intrinsic band bending. No such shift is observed in our system. These data provide essential information, confirming the absence of changes induced by the laser on the bare substrate and allows a direct comparison to

irrefutably attribute any changes observed on the water-covered TiO_2 surface to the presence of water.

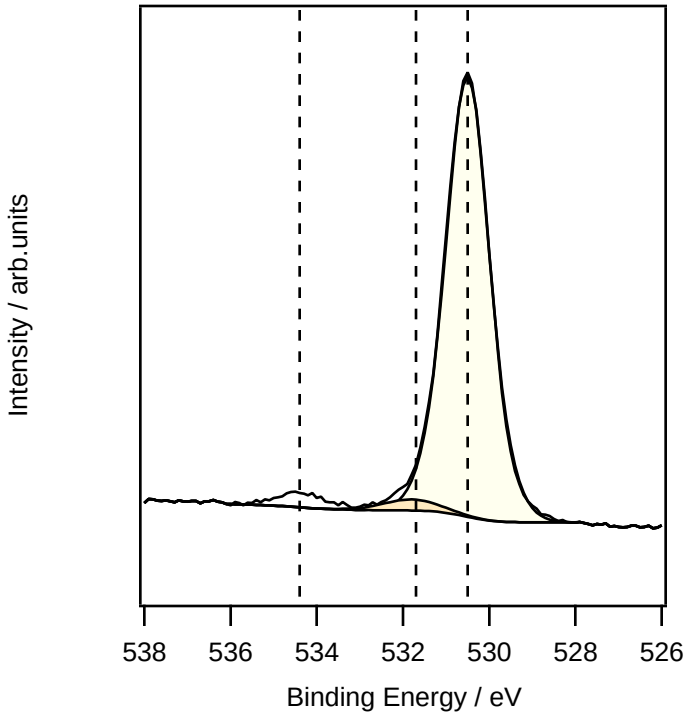

S4: Time averaged data (hν_{FEL} = 645 eV, hν_{opt} = 1.6 eV, T = 160 K) of the O 1s core level which shows a clearer representation of the water coverage during our experiment (Figure 1, in the main text) by averaging over the entire temporal window. Three contributions are present. The peaks at 530.5 eV and 531.8 eV correspond to TiO_2 and TiOH, respectively[30]. The contribution centred at 534.4 eV corresponds to H_2O, with deconvolution thereof discussed in the main text.

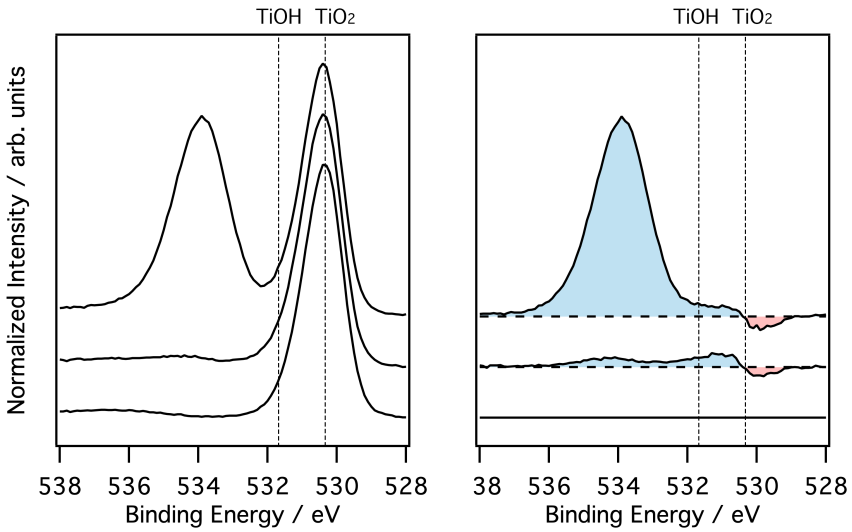

S5: Core level O1s spectra displaying the changes induced following the adsorption of water on the TiO_2 anatase(101) surface. The experiment was carried out using a lab based SPECS XPS instrument at the DESY NanoLab[31] consisting of a monochromatic Al X-ray source ($h\nu = 1486.6$ eV; anode operating at 14 kV) with a high-resolution two-dimensional delay line detector. XP spectra were recorded in fixed transmission mode, with a pass energy of 30 eV, at normal emission within a temperature of 110 K. The data demonstrates that upon water adsorption we observe a positive binding energy shift due to downward band bending with the corresponding formation of TiOH species, as reported in literature. The effect appears to saturate with, or before, monolayer water coverage with no additional shift observed in the upper spectra, in agreement with previous reports.[32–34]

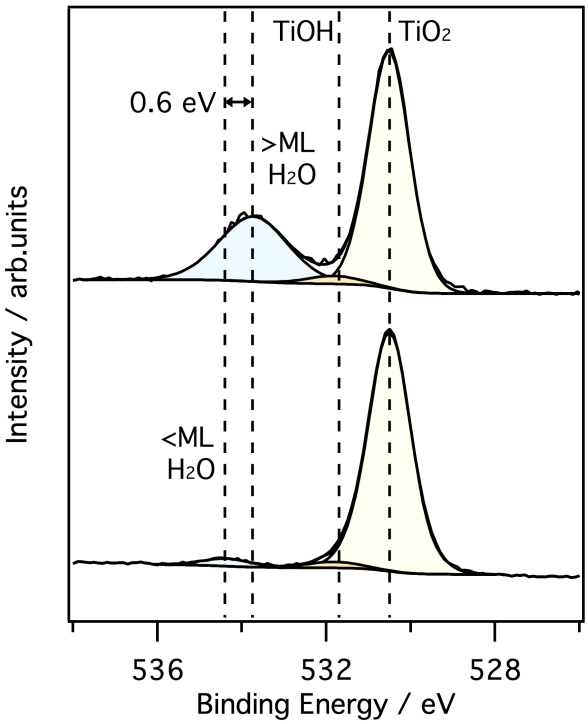

S6: Time averaged data (hν_{FEL} = 645 eV, hν_{opt} = 1.6 eV, T = 110 K (top) and 160 K (bottom)) for the O 1s core level comparing different water coverages. In each case, three contributions are present. The peak located at 530.5 eV corresponds to TiO_2 with a small shoulder at 531.8 eV, corresponding to TiOH. The third peak, though present in both and similarly attributed to molecular water, exhibits a coverage dependent peak shift.[30, 35] At the low coverages present during out experiment the H_2O peak exists at 534.4 eV, as the coverage increases, and ice grows, the peak shifts to 533.8 eV (Δ E = 0.6 eV).

It is widely reported, and similarly shown here, which displays the O 1s core level acquired with different surface coverages of water, that the core level photoemission peak corresponding to molecularly adsorbed water exhibits significant coverage dependent binding energy shifts. For sub-monolayer coverages up until completion of the first (water bound to 5-fold Ti sites) and second (water bound to 2 fold O sites) monolayers a binding energy decrease of 1 eV is reported, both experimentally and theoretically[35, 36]. The precise reason for this shift is not irrefutably known, but a number of possibilities have been proposed including initial state chemical shifts due to a change in the nature of the surface water bonding, final state effects due to changes in the screening caused by either other molecules or the surface and finally due to increases in the hydrogen-oxygen bond length caused by hydrogen bond-

ing with a neighbouring water molecule. The majority of this shift takes place within these first two monolayers and, to a rough approximation, is linear[35]. Using this information in conjunction with Figure S5 we can approximate our water coverage by assuming that the multilayer peak experiences the maximum shift of 1 eV. Thus from the binding energy of the water peak during our experiment (ΔE = 0.6 eV) we can estimate a coverage of around 80% of the first monolayer, i.e. water only bound to 5-fold Ti sites. Since at higher coverages the water peak begins to shift slightly back towards the high binding energy direction, this is likely a small overestimate but is to a good approximation accurate.

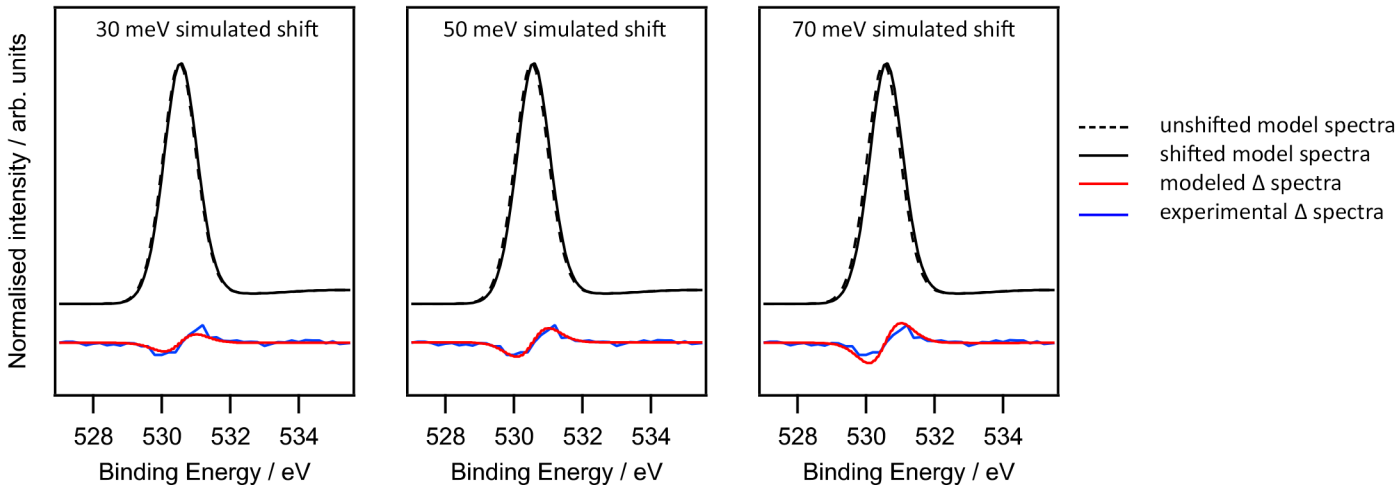

S7: To illustrate the changes that are expected in the differential data due to a rigid band bending induced shift, the model line profile (shown by a dotted line) which was used to fit the time averaged data (Gaussian:Lorentzian;70:30), has been arbitrarily shifted by three different values of 30 meV, 50 meV and 70 meV (displayed as a solid line). The corresponding differential spectra is shown in red and compared to the experimentally observed spectrum in blue. A shift of 50 meV yields an excellent match to our data and is thus our quoted value of the shift. Additionally, this shows that there is no evidence of broadening/changes in peak symmetry in our differential spectra and the main contributing factor to the observed change is a rigid peak shift.

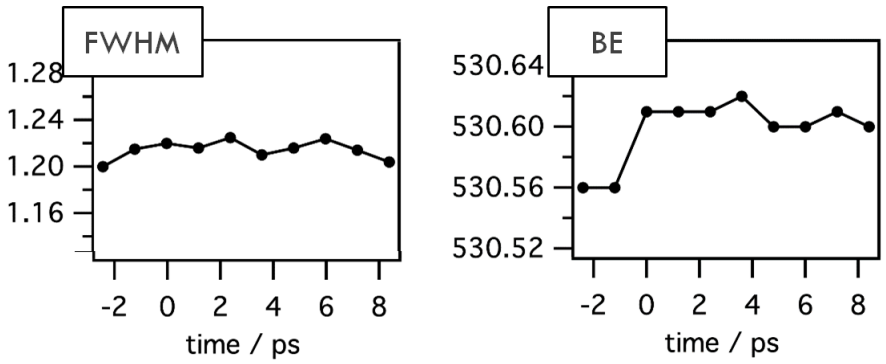

S8: fitting results for the time-resolved O 1s spectra in Figure 1 b in the main text. A consistent shift on the order of 50 meV is observed following laser illumination of water adsorbed TiO_2. No discernible change in the FWHM is observed and the data can be reliably fit with the same line profile. A rigid shift (with no evidence of broadening, or changes in the asymmetry/line profile) of the entire substrate related atomic core level in such a way is indicative of changes in surface band bending. Band bending, which reflects the influence of surface charge on the binding energy of atomic core levels at the interface, is a relatively common phenomena in semiconductors[25]. The depth that is affected by such a phenomenon is typically of the order of 10^{-6} - 10^{-8} m for semiconductors and as such, due to the high surface sensitivity, XPS measures only the affected species and the phenomenon manifests itself as a binding energy shift of the entire core level peak[27]. In our case, based on the observed direction of the O 1s core level shift, it can be inferred that there is an increase in downward band bending. This shift was not observed in the pre-pumped region (< 0 ps) suggesting that it can be attributed to hole transfer from the valence band of TiO_2 to surface adsorbates, immediately following the generation of electron hole pairs induced by the laser. For the sake of a comprehensive discussion, it is also possible that observed shift could be related to the fact that only some surface oxygen atoms change their structural/chemical environment throughout the photoinduced processes. If this is the case, one might not expect a rigid shift of the entire peak but indeed an effective shift, resulting in non-negligible changes in the peak FWHM and symmetry profile. We do not observe this, at least not to a great enough extent to induce the observed core level shift. Thus we believe that we can confidently attribute the changes for the most part to band bending induced shifts. Furthermore, no structural changes of the TiO_2 lattice were seen during the calculations supporting our hypothesis. However, it is nevertheless possible that

such potential changes could contribute to this shift and we are unable to unambiguously rule out a minor role from our experimental data.

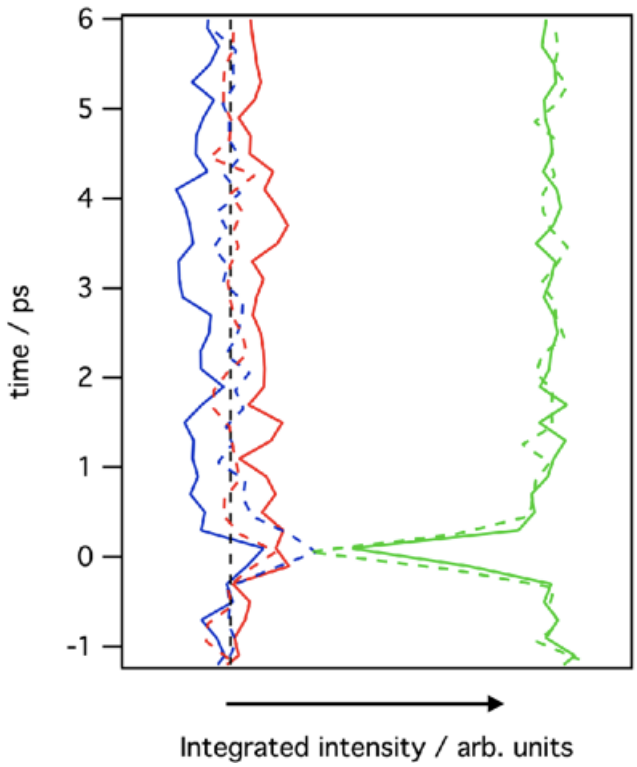

S9: An overlay of two integrated intensity plots to further highlight the fact that the observed shift on the water dosed surface (solid lines) is a real water induced effect and not present on the clean surface (dashed lines). Similarly to the main text, the red and blue lines correspond to intensity integrated over the high and low binding energy sides of the lattice oxide peak, respectively, and the green line is integrated over the peak maximum. The data is extracted over equivalent binding energy windows and averaged over equivalent temporal windows to ensure reliable comparability. Of note is that on the clean surface the laser power was stronger, as evidenced by enhanced sideband formation, so as such it is clear that the change observed on the water dose surface is a consequence of the presence of water since any changes induced by the laser, for example the SPV effect,[7] should be more prominent on the as-prepared surface. In order to ensure the absence of water on the as-prepared surface, spectra were recorded at room temperature. Cooling the system led to the unavoidable adsorption of small amounts of water from the residual vacuum which would skew the data. To shortly address potential concerns surrounding the difference in temperature between the two systems please refer to our previous study in which the photooxidation of CO on TiO_2 was investigated at 60 K using the same experimental setup. The as-prepared surface was also investigated with a higher laser power to ensure the absence of water during the

measurement[5]. Similarly to our system here at room temperature, no core level shifts were observed for the as-prepared surface at colder temperatures allowing us to rule out the change in temperature for any observed differences.

S10: To obtain an accurate understanding of the laser-induced properties of H_2O adsorbed on TiO_2 anatase(101) it is necessary to study several adsorption configurations and the corresponding effect that the geometry has on the photochemistry.

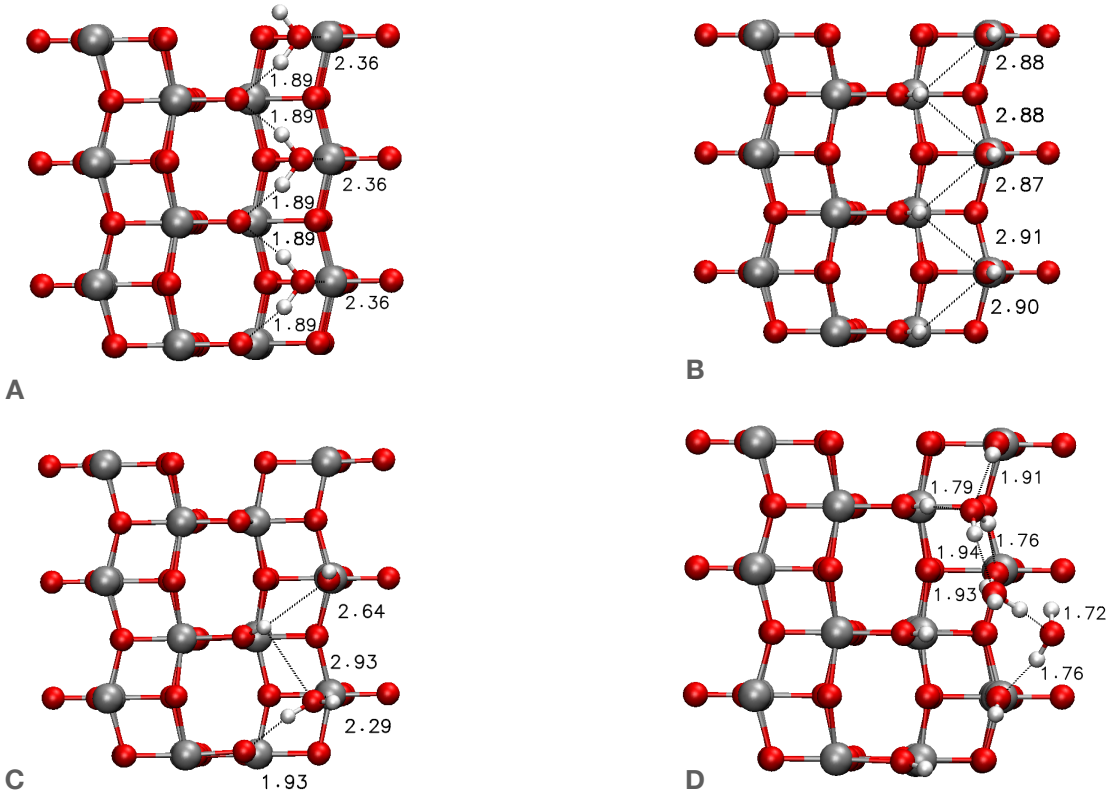

The above Figure includes the molecular representation of a unit cell for the optimized geometry obtained for (A) molecular adsorption (undissociated) of H_2O molecules on TiO_2 anatase(101) surface (B) dissociative adsorption of H_2O molecules on TiO_2 anatase(101) surface (C) a mixture of molecular and dissociative adsorption of H_2O molecules on TiO_2 anatase(101) surface (D) molecular adsorption of H_2O molecules on the hydroxylated TiO_2 anatase(101) surface. Bond lengths are given in angstroms ($\mathring{A}$).

System	E_{ads} **/ eV**
molecular adsorption	-0.85
dissociative adsorption	-0.57
molecular and dissociative adsorption	-0.68
molecular adsorption on a hydroxylated surface	-0.44

TABLE I. Energetic values for the adsorption energies in eV per H_2O adsorbed molecule.

Results obtained for the adsorption energy of water molecules adsorbed over the most stable active site Ti_{5c} (the structural geometry shown) , E_{ads} = -0.85 eV, were found to be in good agreement with theoretical and experimental data for the adsorption of water on TiO_2 anatase (101).[12, 37, 38] The system with both molecular and dissociative adsorption, E_{ads} = -0.68 eV, is a more stable configuration when compared to the dissociatively adsorbed system and molecular adsorption over a fully hydroxylated surface, in agreement with previous reports[39]. This is the system we experimentally observed, see S4. For the hydroxylated systems the Ti_{5c}-OH bond distance is 1.90 $\mathring{A}$ and there is a bond distance expansion for Ti_{5c}-O_{2c} in accordance with literature.[14]

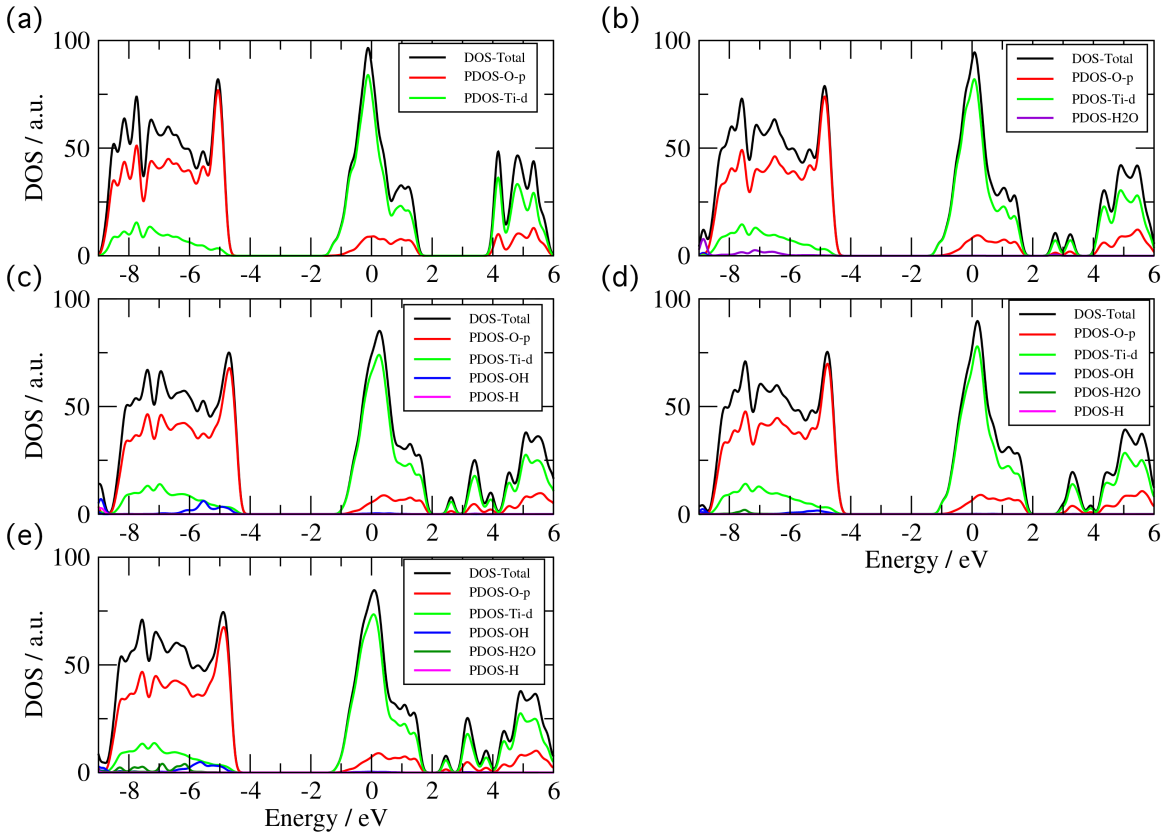

S11: Here, the density of States (DOS) and Partial Density of States (PDOS) for the corresponding systems are displayed. (a) represents the clean TiO_2 anatase 101 surface. (b) represents the undissociated water adsorbed system. (c) corresponds to the dissociated water adsorbed system. (d) corresponds to undissociated water adsorbed over Ti_{5c} sites and partially hydroxylated surface. (e) corresponds to undissociated water adsorbed over a fully hydroxylated surface.

In the DOS of the TiO_2 anatase(101) surface the valence band is predominantly O 2p character with a minor presence of hybridized Ti 3d states. The conduction band is predominantly Ti 3d character with a minor presence of hybridized O 2p states. No significant changes appear when H_2O molecules adsorb molecularly (undissociated). Importantly, the dissociatively adsorbed molecules present significant hybridization of the OH terminal group with the O 2p states of the surface at the top of the valence band.

	H_2O	TiOH	TiO_2
Mixed	545.0	542.1	541.4
Undissociated	544.3 544.4	-	541.4
Exp.	534.4	531.8	530.5

S12: Calculated O 1s core level XPS binding energies pertaining to H_2O adsorbed on anatase TiO_2(101). The VASP code[15–18] was employed. Calculations were carried out at the Γ point and using PBE functional[19] with an energy cutoff of 450 eV and the projected augmented-wave method[20, 21]. To calculate the core level energies the Slater transition state approach was selected.

Note that the absolute values of the binding energies cannot be accurately predicted within the VASP implementation of the projector augmented wave method[40], but the relative shifts can provide meaningful information. The theoretical results are similar to the findings in the experimental XPS. A shift relative to the substrate TiO_2 component of the O1s core level is found for the peaks corresponding to TiOH and molecularly adsorbed H_2O. This is shown below for two configurations; mixed molecular and dissociative adsorption of H_2O molecules on TiO_2 anatase(101) (left) and molecular adsorption (undissociated) of H_2O molecules on TiO_2 anatase(101) surface (right). O_a, O_b,O_c atom types are referred in the Table as TiO_2, Ti-OH, and molecular H_2O, respectively. Also included are the experimentally observed values for comparison.

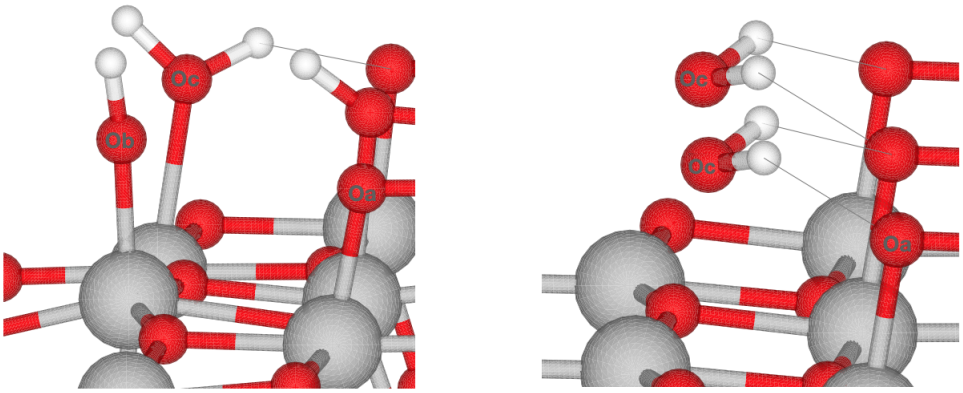

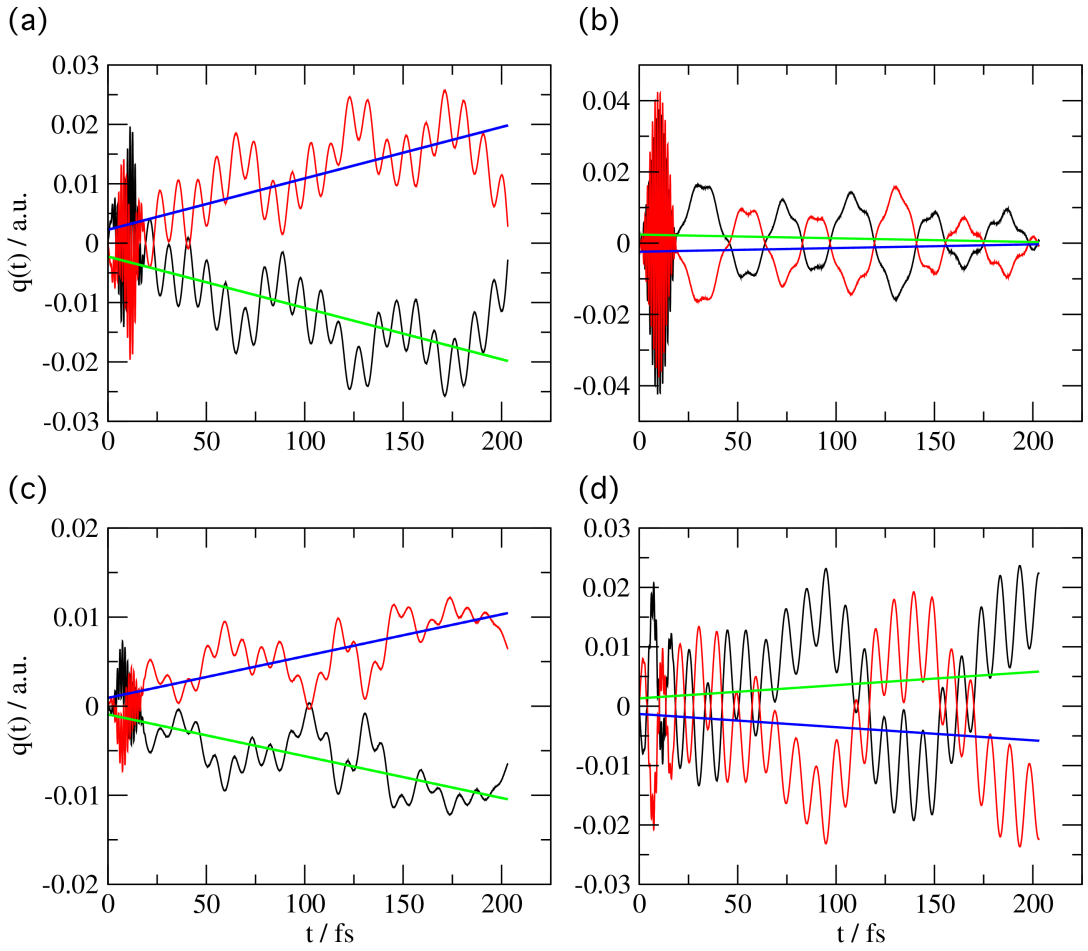

S13: The initial dynamics ruling this charge-transfer process are studied in an Ehrenfest dynamics simulation using the energy value for a laser pulse of 382 nm (3.245 eV) with a total pulse duration of 20 fs. The figure displays the changes in the Mulliken charges with respect to their ground-state values as a function of time for the systems under study. (a) represents the undissociated water adsorbed system. (b) represents the dissociative water adsorbed system. (c) corresponds with undissociated water adsorbed over Ti_{5c} site and partially hydroxylated surface. (d) corresponds with undissociated water adsorbed over a fully hydroxylated surface. The black and red lines correspond to the instantaneous charge of the surface and the H_2O molecules respectively, with the green and blue lines representing an average value of the charge for the surface and the H_2O molecules respectively. The adsorption configuration of H_2O has a significant effect on the photo-induced charge transfer processes on the TiO_2 anatase(101) surface.

For the systems with complete dissociative adsorption and molecular adsorption on a

complete hydroxylated surface, the charge transfer is displayed from the surface to the H_2O molecules. These configurations are the two least stable ones from a thermodynamics point of view, shown in Table 1. The charge-transfer evolution in these two cases underlines the presence of an excess of electrons at the surface favouring reduction processes. A similar conclusion was discussed by A. Selloni et al.[41] For the two most stable configurations, the molecular adsorption and a mixed molecular and dissociated adsorption, a net charge transfer from water molecules to the TiO_2 surface is observed immediately during the simulation.

	$\mathbf{BE}_{TiO_2}$ / **eV**			$\mathbf{BE}_{H_2O}$ / **eV**		
	$\mathbf{t<t_0}$	$\mathbf{t>t_0}$	Δ	$\mathbf{t<t_0}$	$\mathbf{t>t_0}$	Δ
experiment	530.45	530.50	0.05	534.61	534.0	-0.61
theory	541.4	541.5	0.1	545.0	544.1	-0.9

S14: Calculated and experimental binding energies for the O 1s photoelectron before (geometry configuration (a) in Figure 3 in the main text) and after (geometry configuration (d) in Figure 3 in the main text) illumination. Calculations were done for the mixed configuration using the VASP code[15–18] and the Kohn Sham half occupied core state energies

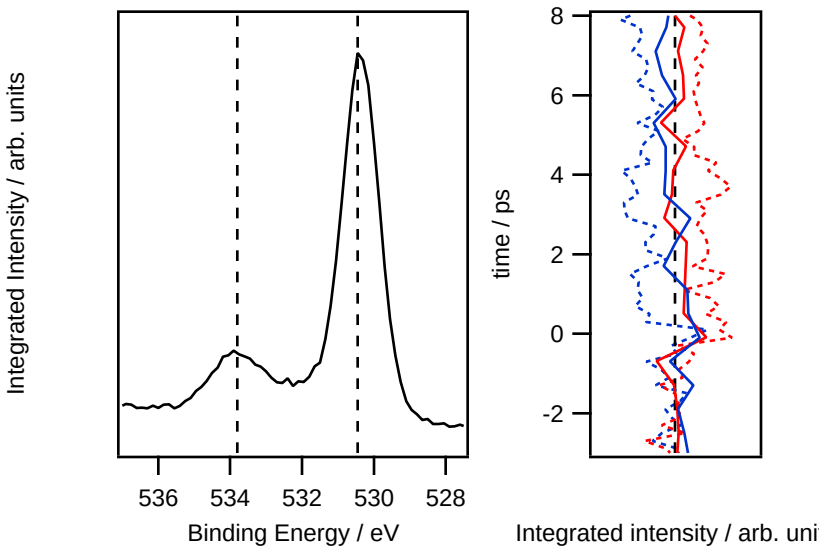

S15: Core level O1s spectra displaying the time averaged data averaged over the entire temporal window (hν_{FEL} = 645 eV, hν_{opt} = 1.6 eV, T = 150 K) which shows a higher water coverage during our experiment to allow a preliminary investigation into the effect of water coverage on the surface photochemistry. Data was recorded at a slightly lower temperature of 150 K (to allow coverage to be controlled) with otherwise equivalent experimental conditions and laser parameters. The lattice oxide peak is located at 530.5 eV with the H_2O component at 533.8 eV. As discussed in S5 it is known that that the core level photoemission peak associated with molecularly adsorbed water exhibits significant coverage dependent binding energy shifts for sub-monolayer coverages up until completion of the first (water bound to 5-fold Ti sites) and second (water bound to 2 fold O sites) monolayers[35, 36]. In this case we observe the maximum shift and so can clarify that here we have >ML coverage. This is nevertheless clear from a comparison of relative intensities to Figure S4.

Similarly to previous spectra, the temporal changes of the O 1s core level that are induced following laser illumination are shown to the right. For direct comparison the data at lower coverages from the main text is included as dashed lines. Similarly to the main text, the red and blue lines correspond to intensity integrated over the high and low binding energy sides of the lattice oxide peak, respectively, as a function of delay time. The data is extracted over equivalent binding energy windows but the higher coverage data is averaged over a larger temporal window (0.6 ps) to ensure a comparable signal-to-noise ratio due to reduced data acquisition times. Unlike at lower coverages, no discernible changes are observed. At

higher water coverages the peak position remains constant upon laser illumination and no broadening takes place suggesting that at higher coverages the photochemistry at the surface differs. This is discussed in the main text.

---

* Corresponding author: michael.wagstaffe@desy.de

† Corresponding author: andreas.stierle@desy.de

[1] M. Martins, M. Wellhöfer, J. T. Hoeft, W. Wurth, J. Feldhaus, and R. Follath, Monochromator beamline for FLASH, Review of Scientific Instruments **77**, 115108 (2006).

[2] N. Gerasimova, S. Dziarzhytski, and J. Feldhaus, The monochromator beamline at FLASH: performance, capabilities and upgrade plans, Journal of Modern Optics **58**, 1480 (2011).

[3] S. Toleikis, The FLASH facility current status in 2018 and future upgrade plans, AIP Conference Proceedings **2054**, 030015 (2019).

[4] W. Ackermann, G. Asova, V. Ayvazyan, A. Azima, N. Baboi, J. Bähr, V. Balandin, B. Beutner, A. Brandt, A. Bolzmann, R. Brinkmann, O. I. Brovko, M. Castellano, P. Castro, L. Catani, E. Chiadroni, S. Choroba, A. Cianchi, J. T. Costello, D. Cubaynes, J. Dardis, W. Decking, H. Delsim-Hashemi, A. Delserieys, G. Di Pirro, M. Dohlus, S. Düsterer, A. Eckhardt, H. T. Edwards, B. Faatz, J. Feldhaus, K. Flöttmann, J. Frisch, L. Fröhlich, T. Garvey, U. Gensch, C. Gerth, M. Görler, N. Golubeva, H. J. Grabosch, M. Grecki, O. Grimm, K. Hacker, U. Hahn, J. H. Han, K. Honkavaara, T. Hott, M. Hüning, Y. Ivanisenko, E. Jaeschke, W. Jalmuzna, T. Jezynski, R. Kammering, V. Katalev, K. Kavanagh, E. T. Kennedy, S. Khodyachykh, K. Klose, V. Kocharyan, M. Körfer, M. Kollewe, W. Koprek, S. Korepanov, D. Kostin, M. Krassilnikov, G. Kube, M. Kuhlmann, C. L. S. Lewis, L. Lilje, T. Limberg, D. Lipka, F. Löhl, H. Luna, M. Luong, M. Martins, M. Meyer, P. Michelato, V. Miltchev, W. D. Möller, L. Monaco, W. F. O. Müller, O. Napieralski, O. Napoly, P. Nicolosi, D. Nölle, T. Nuñez, A. Oppelt, C. Pagani, R. Paparella, N. Pchalek, J. Pedregosa-Gutierrez, B. Petersen, B. Petrosyan, G. Petrosyan, L. Petrosyan, J. Pflüger, E. Plönjes, L. Poletto, K. Pozniak, E. Prat, D. Proch, P. Pucyk, P. Radcliffe, H. Redlin, K. Rehlich, M. Richter, M. Roehrs, J. Roensch, R. Romaniuk, M. Ross, J. Rossbach, V. Rybnikov, M. Sachwitz, E. L. Saldin, W. Sandner, H. Schlarb, B. Schmidt, M. Schmitz, P. Schmüser, J. R. Schneider, E. A. Schneidmiller, S. Schnepp, S. Schreiber, M. Seidel, D. Sertore, A. V. Shabunov, C. Si-

mon, S. Simrock, E. Sombrowski, A. A. Sorokin, P. Spanknebel, R. Spesyvtsev, L. Staykov, B. Steffen, F. Stephan, F. Stulle, H. Thom, K. Tiedtke, M. Tischer, S. Toleikis, R. Treusch, D. Trines, I. Tsakov, E. Vogel, T. Weiland, H. Weise, M. Wellhöfer, M. Wendt, I. Will, A. Winter, K. Wittenburg, W. Wurth, P. Yeates, M. V. Yurkov, I. Zagorodnov, and K. Zapfe, Operation of a free-electron laser from the extreme ultraviolet to the water window, Nature Photonics **1**, 336 (2007).

[5] M. Wagstaffe, L. Wenthaus, A. Dominguez-Castro, S. Chung, G. D. Lana Semione, S. Palutke, G. Mercurio, S. Dziarzhytski, H. Redlin, N. Klemke, Y. Yang, T. Frauenheim, A. Dominguez, F. Kärtner, A. Rubio, W. Wurth, A. Stierle, and H. Noei, Ultrafast real-time dynamics of co oxidation over an oxide photocatalyst, ACS Catalysis **10**, 13650 (2020).

[6] M. Watanabe and T. Hayashi, Time-resolved study of self-trapped exciton luminescence in anatase TiO_2 under two-photon excitation, Journal of Luminescence **112**, 88 (2005).

[7] K. Ozawa, M. Emori, S. Yamamoto, R. Yukawa, S. Yamamoto, R. Hobara, K. Fujikawa, H. Sakama, and I. Matsuda, Electron-hole recombination time at TiO_2 single-crystal surfaces: influence of surface band bending, The Journal of Physical Chemistry Letters **5**, 1953 (2014).

[8] L. Wenthaus, A. Benz, S. Palutke, D. Kutnyakhov, H. Meyer, S. Gieschen, and M. Beye, Double electron spectrometer setup for time-resolved photoelectron spectroscopy at a free-electron laser, in preparation (2021).

[9] U. Diebold, The surface science of titanium dioxide, Surface Science Reports **48**, 53 (2003).

[10] P. K. Samanta and N. J. English, Opto-electronic properties of stable blue photosensitisers on a TiO_2 anatase-101 surface for efficient dye-sensitised solar cells, Chemical Physics Letters **731**, 136624.

[11] B. Aradi, B. Hourahine, and T. Frauenheim, DFTB+, a sparse matrix-based implementation of the DFTB method, The Journal of Physical Chemistry A **111**, 5678 (2007).

[12] D. Selli, G. Fazio, G. Seifert, and C. Di Valentin, Water multilayers on TiO_2(101) anatase surface: Assessment of a DFTB-based method, Journal of Chemical Theory and Computation **13**, 3862 (2017).

[13] F. P. Bonafé, B. Aradi, M. Guan, O. A. Douglas-Gallardo, C. Lian, S. Meng, T. Frauenheim, and C. G. Sánchez, Plasmon-driven sub-picosecond breathing of metal nanoparticles, Nanoscale **9**, 12391 (2017).

[14] F. P. Bonafé, F. J. Hernández, B. Aradi, T. Frauenheim, and C. G. Sánchez, Fully atomistic

real-time simulations of transient absorption spectroscopy, The Journal of Physical Chemistry Letters **9**, 4355 (2018).

[15] G. Kresse and J. Furthmüller, Efficiency of ab-initio total energy calculations for metals and semiconductors using a plane-wave basis set, Computational Materials Science **6**, 15 (1996).

[16] G. Kresse and J. Furthmüller, Efficient iterative schemes for ab initio total-energy calculations using a plane-wave basis set, Physical Review B **54**, 11169 (1996).

[17] G. Kresse and J. Hafner, Ab initio molecular dynamics for liquid metals, Physical Review B **47**, 558 (1993).

[18] G. Kresse and J. Hafner, Ab initio molecular-dynamics simulation of the liquid-metal–amorphous-semiconductor transition in germanium, Physical Review B **49**, 14251 (1994).

[19] J. P. Perdew, M. Ernzerhof, and K. Burke, Rationale for mixing exact exchange with density functional approximations, The Journal of Chemical Physics **105**, 9982 (1996).

[20] P. E. Blöchl, Projector augmented-wave method, Physical Review B **50**, 17953 (1994).

[21] G. Kresse and D. Joubert, From ultrasoft pseudopotentials to the projector augmented-wave method, Physical Review B **59**, 1758 (1999).

[22] A. Pietzsch, A. Föhlisch, M. Beye, M. Deppe, F. Hennies, M. Nagasono, E. Suljoti, W. Wurth, C. Gahl, K. Döbrich, and A. Melnikov, Towards time resolved core level photoelectron spectroscopy with femtosecond X-ray free-electron lasers, New Journal of Physics **10**, 033004 (2008).

[23] J. O'Connor, B. A. Sexton, and R. S. C. Smart, *Surface Analysis Methods in Materials Science*, Vol. 23 (Springer, 2003).

[24] M. P. Seah and W. A. Dench, Quantitative electron spectroscopy of surfaces: A standard data base for electron inelastic mean free paths in solids, Surface and Interface Analysis **1**, 2.

[25] Z. Zhang and J. T. Yates, Band bending in semiconductors: Chemical and physical consequences at surfaces and interfaces, Chemical Reviews **112**, 5520 (2012).

[26] J. Schneider, M. Matsuoka, M. Takeuchi, J. Zhang, Y. Horiuchi, M. Anpo, and D. W. Bahnemann, Understanding TiO_2 photocatalysis: Mechanisms and materials, Chemical Reviews **114**, 9919 (2014).

[27] C. T. Campbell, Ultrathin metal films and particles on oxide surfaces: structural, electronic and chemisorptive properties, Surface Science Reports **27**, 1 (1997).

[28] K. L. Syres, A. G. Thomas, W. R. Flavell, B. F. Spencer, F. Bondino, M. Malvestuto, A. Pre-

obrajenski, and M. Grätzel, Adsorbate-induced modification of surface electronic structure: Pyrocatechol adsorption on the anatase TiO_2 (101) and rutile TiO_2 (110) surfaces, The Journal of Physical Chemistry C **116**, 23515 (2012).

[29] Y. Zhang, D. T. Payne, C. L. Pang, C. Cacho, R. T. Chapman, E. Springate, H. H. Fielding, and G. Thornton, State-selective dynamics of TiO_2 charge-carrier trapping and recombination, The Journal of Physical Chemistry Letters **10**, 5265 (2019).

[30] M. J. Jackman, A. G. Thomas, and C. Muryn, Photoelectron spectroscopy study of stoichiometric and reduced anatase TiO_2(101) surfaces: the effect of subsurface defects on water adsorption at near-ambient pressures, The Journal of Physical Chemistry C **119**, 13682 (2015).

[31] A. Stierle, T. F. Keller, H. Noei, V. Vonk, and R. Roehlsberger, Desy nanolab, Journal of large-scale research facilities **2** (2016).

[32] L. E. Walle, A. Borg, E. M. J. Johansson, S. Plogmaker, H. Rensmo, P. Uvdal, and A. Sandell, Mixed dissociative and molecular water adsorption on anatase TiO_2(101), The Journal of Physical Chemistry C **115**, 9545 (2011).

[33] M. B. Hugenschmidt, L. Gamble, and C. T. Campbell, The interaction of H_2O with a TiO_2(110) surface, Surface Science **302**, 329 (1994).

[34] S. Kashiwaya, J. Morasch, V. Streibel, T. Toupance, W. Jaegermann, and A. Klein, The work function of TiO_2, Surfaces **1**, 73 (2018).

[35] G. S. Herman, Z. Dohnálek, N. Ruzycki, and U. Diebold, Experimental investigation of the interaction of water and methanol with anatase-TiO_2(101), The Journal of Physical Chemistry B **107**, 2788 (2003).

[36] P. Aplincourt, C. Bureau, J.-L. Anthoine, and D. P. Chong, Accurate density functional calculations of core electron binding energies on hydrogen-bonded systems, The Journal of Physical Chemistry A **105**, 7364 (2001).

[37] S. Rhatigan and M. Nolan, Activation of water on MnO_x-nanocluster-modified rutile (110) and anatase (101) TiO_2 and the role of cation reduction, Frontiers in Chemistry **7**, 67 (2019).

[38] D. D. Beck, J. M. White, and C. T. Ratcliffe, Catalytic reduction of carbon monoxide with hydrogen sulfide. 2. adsorption of water and hydrogen sulfide on anatase and rutile, The Journal of Physical Chemistry **90**, 3123 (1986).

[39] R. Martinez-Casado, G. Mallia, N. M. Harrison, and R. Pérez, First-principles study of the water adsorption on anatase(101) as a function of the coverage, The Journal of Physical

Chemistry C **122**, 20736 (2018).

[40] N. Pueyo Bellafont, F. Viñes, W. Hieringer, and F. Illas, Predicting core level binding energies shifts: Suitability of the projector augmented wave approach as implemented in VASP, Journal of Computational Chemistry **38**, 518 (2017).

[41] S. Selcuk and A. Selloni, Facet-dependent trapping and dynamics of excess electrons at anatase TiO_2 surfaces and aqueous interfaces, Nature Materials **15**, 1107 (2016).